Electronic Supplementary Information (ESI)

Evidence of Catalyzed Oxidation of Li_2O_2 for Rechargeable Li-Air Battery Applications

Jonathon R. Harding,[a] Yi-Chun Lu,[b] Yasuhiro Tsukada,[c] and Yang Shao-Horn*[b,c]

a Department of Chemical Engineering, Massachusetts Institute of Technology, 77 Massachusetts Avenue, Cambridge, MA 02139, USA
b Department of Materials Science and Engineering, Massachusetts Institute of Technology, 77 Massachusetts Avenue, Cambridge, MA 02139, USA
c Department of Mechanical Engineering, Massachusetts Institute of Technology, 77 Massachusetts Avenue, Cambridge, MA 02139, USA

* *shaohorn@mit.edu*

1. Calculation of active carbon normalized capacity and current from McCloskey et al

In McCloskey et al[1], most results are given on an absolute scale of current and capacity, which makes comparison between their results and other published results challenging. In the supplemental information of that paper, the authors give an approximate value of the carbon loading present in their carbonate free electrodes, reporting that the active cathode material ranged from 3-6 mg in each electrode. The authors define active material as both the carbon and catalyst included in the electrode mass.

Assuming a mass of 3 mg of carbon was added to each electrode on average, and observing that each cell was allowed to discharge to 0.4 mAh in 1,2-dimethoxyethane (DME) gives a result of only 130 mAh/g_{carbon}. This value is significantly below the observed capacity of most lithium-oxygen (Li-O_2) cells,[2-4] and any OER activity observed from such experiments may only be representative of the very initial charging behaviour of Li-O_2 cells.

2. Confirmation of Li_2O_2 Purity

The manufacturer reported 90% phase purity of the Li_2O_2 used in this work. XRD was performed on the Li_2O_2 powder both as-purchased and after the ball milling treatment (Fig. S1). The as-purchased powder shows a ~10% phase impurity of LiOH, although the small size of the LiOH peaks and their close proximity to major Li_2O_2 peaks increases the uncertainty of this calculation. Post-ball-milling, only the (200) LiOH peak is detected, and its area is consistent with a 4% LiOH phase impurity. However, the authors are not aware of a reasonable pathway for the conversion of LiOH into Li_2O_2 while dry ball-milling under argon. We propose that the LiOH was present on the surface of the as-purchased Li_2O_2 powder, where ball-milling most effectively reduced LiOH crystal size, thereby reducing its peaks below the XRD detection limit.

For the purposes of estimating the expected cell capacity, this contamination is neglected. The number of Li atoms present changes by only 0.3% by including a 10% LiOH impurity. Additionally, the thermodynamic equilibrium potential for LiOH is 3.3 V vs Li, below the operating potential of all cells presented here. We therefore assume that LiOH is also oxidized during charging, which is consistent with the agreement between the observed and expected capacities.

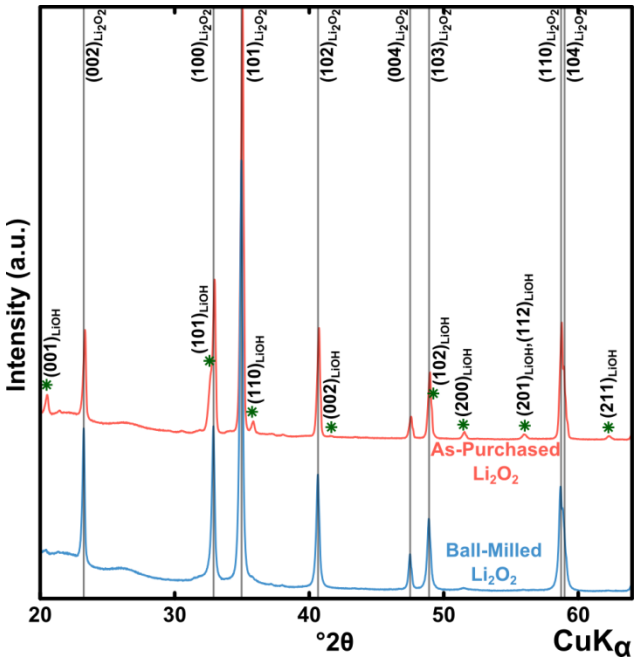

Fig. S1: XRD spectra of Li_2O_2 powder as-purchased and after ball-milling. Grey vertical lines denote Li_2O_2 lattice planes, and green stars denote LiOH lattice planes.

3. Example calculation of Potentiostatic Net Current, Capacity, and Activity

Potentiostatic net current was calculated by subtracting the carbon mass normalized background current from the carbon mass normalized current of Li_2O_2-containing cells. Capacity was calculated by integrating the net Li_2O_2 oxidation current with respect to time. This process is shown graphically in Fig. S2.

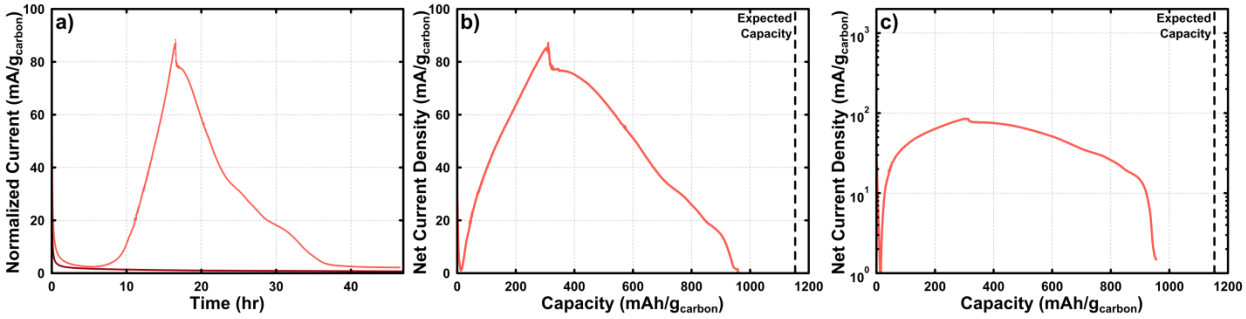

Fig. S2: Example background subtraction and capacity integration for an Au/C+Li_2O_2 cell charged at 4.3 V. (a) Carbon normalized active and background current vs. time, (b) Background subtracted net current vs. time, (c) Net current vs. capacity on a linear scale, and (d) Net current vs. capacity on a log scale as presented in the paper.

4. SEM and Particle Size Analysis of Ball-Milled Li_2O_2

Ball-milled Li_2O_2 was observed under SEM to collect a particle size distribution. Two-axis measurements of particle length was taken for each particle in Fig. S3a, and combined to generate the equivalent circular diameter for each particle. The distribution of particle sizes is plotted in Fig. S3b, with the mean size being 345 nm.

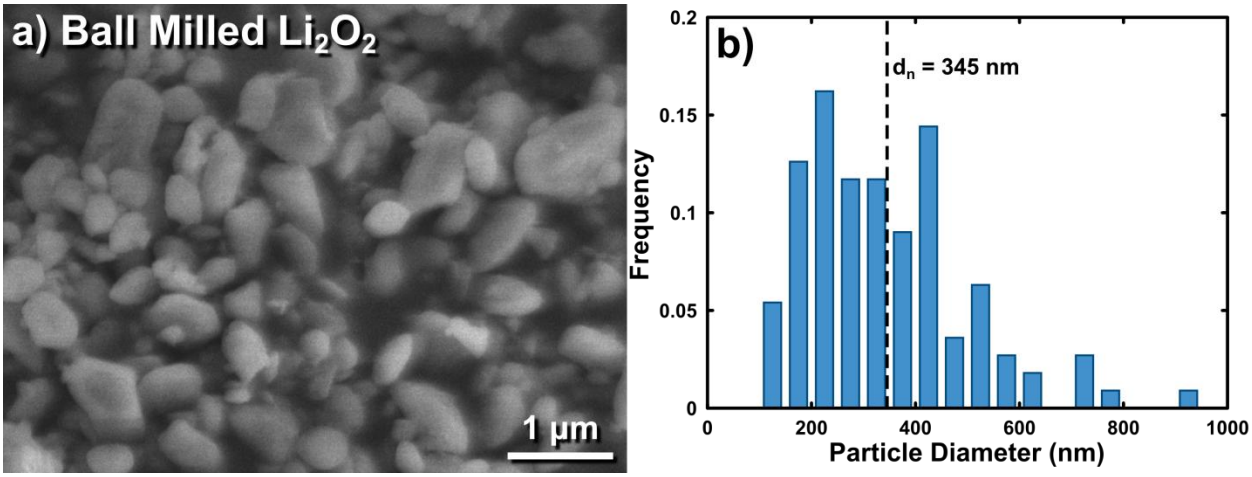

Fig. S3: (a) SEM of ball-milled Li_2O_2. (b) Particle size distribution of particles present in (a).

5. TEM of Vulcan Carbon Supported Catalysts

TEM of the catalysts used in this paper was collected, and is presented in Fig. S4. Au nanoparticles were significantly larger than the Pt and Ru particles, reaching a ~13 nm average diameter, versus 2 and 3 nm for Pt and Ru respectively.

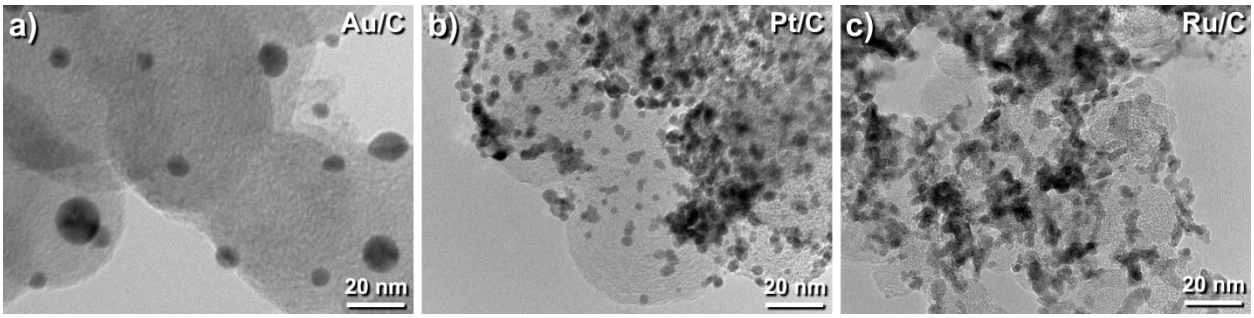

Fig. S4: TEM of VC supported catalyst. (a) Au on XC72 Vulcan carbon (Au/C), (b) Pt on XC72 Vulcan carbon (Pt/C), (c) Ru on XC72 Vulcan carbon (Ru/C).

6. Relationship between Li_2O_2 Peak Size and Charge Capacity

For each catalyst, XRD was performed on pristine, ~50% charged, and 100% charged electrodes (Fig. S5). The size of the Li_2O_2 diffraction peaks was observed to reduce in size consistently with increasing cell charging. Fig. S5 shows the percent reduction in the primary $(101)_{Li2O2}$ peak area (relative to the pristine electrode) against the % of the observed cell capacity. The observed capacities used were 1050 mAh/g_{carbon} (VC+Li_2O_2), 1300 mAh/g_{carbon} (Au/C+Li_2O_2), 900 mAh/g_{carbon} (Pt/C+Li_2O_2), and 1150 mAh/g_{carbon} (Ru/C+Li_2O_2). Vulcan C+Li_2O_2 and Pt/C+Li_2O_2 were consistent with a 1:1 relationship between area and capacity for all three points, while Au/C+Li_2O_2 and Ru/C+Li_2O_2 were found to have a slightly higher Li_2O_2 peak area than expected after ~50% charge.

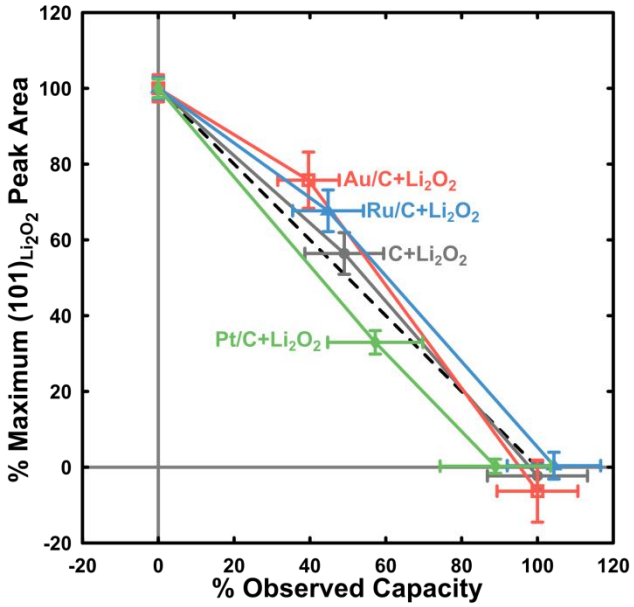

Fig. S5: Percent reduction of the $(101)_{Li2O2}$ diffraction peak area vs. percent observed capacity for VC+Li_2O_2, Au/C+Li_2O_2, Pt/C+Li_2O_2, and Ru/C+Li_2O_2. The dashed black line marks the ideal 1:1 relationship between increasing charging and peak area reduction.

7. Li-O_2 Cell Measurement with Pt/C

An Li-O_2 cell consisting of a lithium metal anode (15 mm in diameter and ~0.45 mm thickness) and a lithiated Nafion®-bonded air electrode (12.7 mm in diameter) of Pt/C was discharged and charged at 100 mAh/g_{carbon}. A detailed description for the preparation and testing of this cell can be found in the experimental section of Lu et al.[3] The first discharge and charge profiles of a Pt/C cell is shown in Fig. S6.

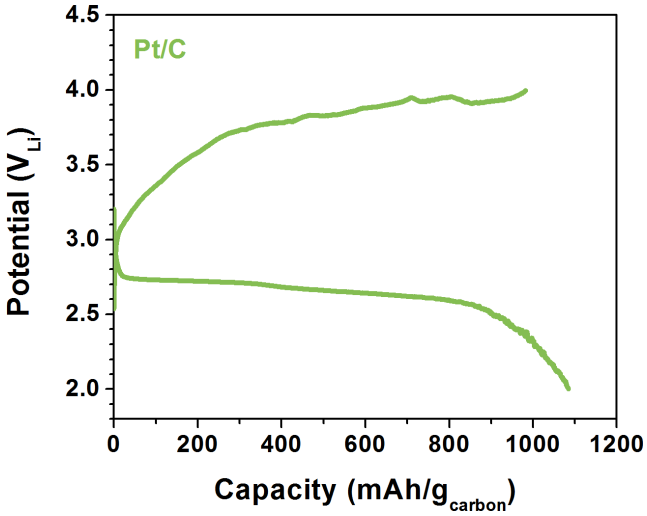

Fig. S6: Discharge and charge profiles of Pt/C in an Li-O_2 cell at 100 mA/g_{carbon}

8. SEM of Charged Electrodes

Scanning electron microscopy (SEM) was performed on some of the charged electrodes containing catalyst (Fig. S7). No peroxide was observed in any fully charged electrode.

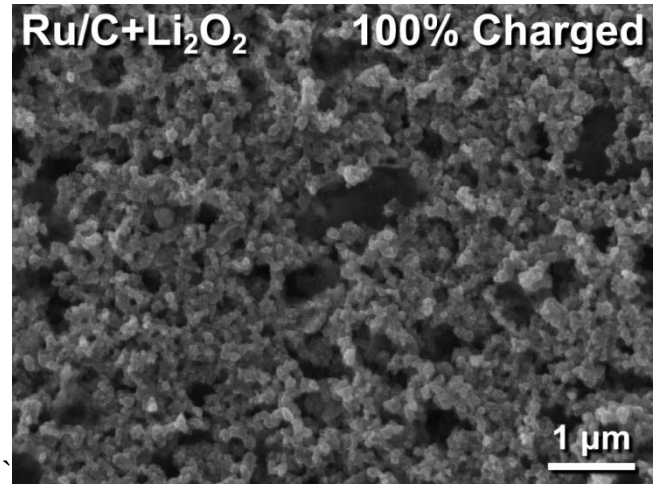

Fig. S7: SEM of a fully charged Ru/C+Li_2O_2 electrode. No Li_2O_2 is visible, and holes in the carbon structure indicate where Li_2O_2 was originally located.

9. Example Calculation of Cell Activity

Using the same cell as displayed above, we also show how activity was calculated in Fig. S8. This was completed by integrating the current with respect to capacity over the first 20% of capacity, then dividing by the width of the capacity region integrated over. Note that the charts below use the same log-log scale presented elsewhere in the paper, so the average value appears weighted towards the top of the integral.

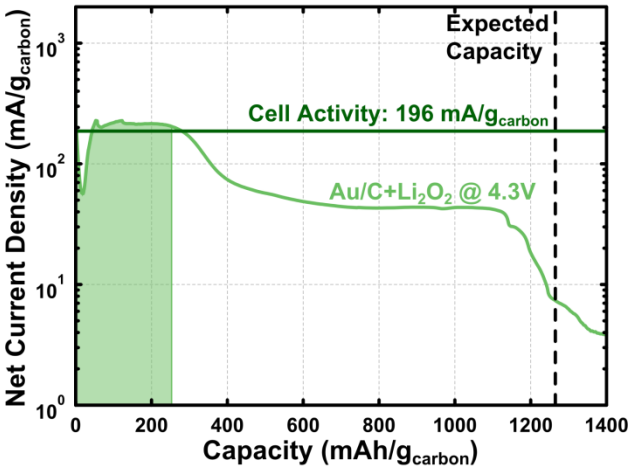

Fig. S8: Example integration process for calculating cell activity for an example Au/C+Li_2O_2 cell at 4.3V.

10. Numerical Fit of Initiation of Li_2O_2 Oxidation

Table S1 provides the fitting parameters (used in Equation 1) and the R^2 value used to fit the VC+Li_2O_2 cells presented in Fig. 9. The fit was calculated using the logarithm of current to prevent overweighting of high-current behaviors. Sampling points were evenly distributed between the decay and rise portions of the current profile, and distributed logarithmically with time in each region.

Potential (V_{Li})	a	b	c	t_0	R^2
4.4	7.4×10^{4}	130	1.7×10^{-5}	660	99.0%
4.3	4.1×10^{4}	180	1.7×10^{-7}	2100	99.5%
4.2	1.5×10^{4}	210	1.2×10^{-10}	5300	96.7%
4.1	1.4×10^{4}	420	1.3×10^{-12}	16000	99.7%

Table S1: Fitting parameters and goodness of fit for Equation 1 on the cells shown in Figure 6.

The value of t_0 was found to decrease exponentially with increasing potential. The value of t_0 for the four points listed in Table S1 are shown in Fig. S9.

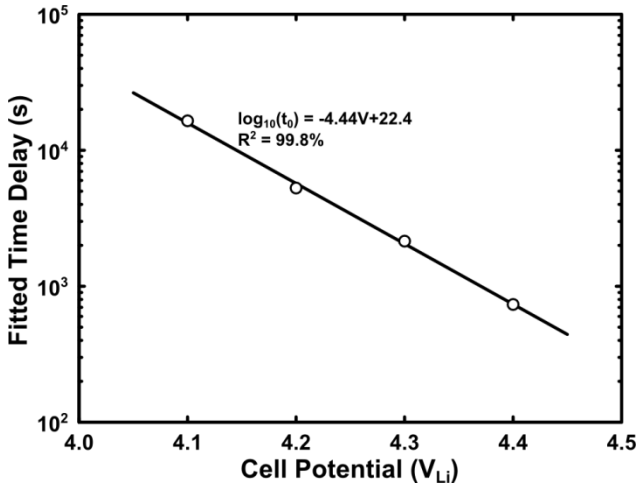

Fig. S9: Fitted time delay vs. charged cell potential for the four cells presented in Table S1.

11. Galvanostatic Results

In addition to potentiostatic testing, a small set of galvanostatic tests were performed. These were completed by charging the cell at a set current, which was later normalized to the carbon mass. Fig. S10 shows the results of these tests on VC+Li_2O_2 electrodes. The cells were able to charge at lower potentials than in purely potentiostatic tests, but also exhibited a large potential spike for the first 10% of charging. It is hypothesized that the large, early potential

activates more nucleation sites than would occur potentiostatically, thereby enabling more Li_2O_2 decomposition to occur at lower potentials.

At moderate currents, such as 500 mA/g_{carbon}, which was regularly exceeded during potentiostatic testing, cells were observed to auto-terminate immediately after the initial voltage spike. This was observed repeatedly and consistently at the same location. This behaviour severely limited the usefulness of these galvanostatic tests.

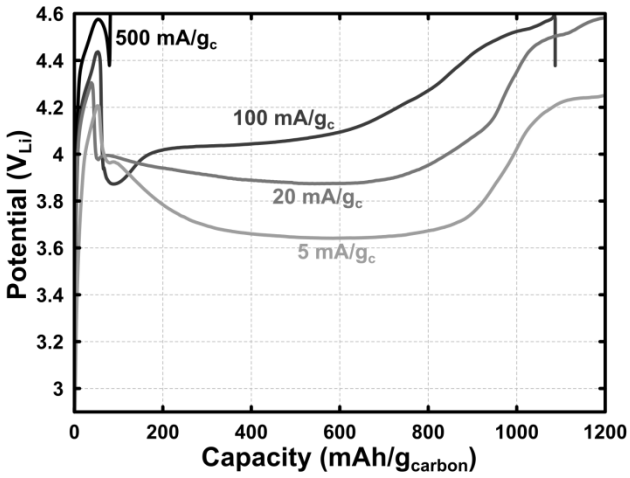

Fig. S10: Potential vs. capacity for galvanostatic charging of VC+Li_2O_2 electrodes. All currents were normalized with respect to carbon mass.

12. Variation of current over time for all catalysts

Net current vs. time is plotted in Fig. S11 for the all catalyst-containing electrodes. Au/C electrodes show a similar trend to that of VC: a dip and rise occurs at the beginning of charging, and the depth and duration of this dip is strongly dependent on the charging voltage. For Pt/C and Ru/C cells, this profile significantly changes, showing a generally downward trend over the entire discharge, with no clear and consistent minimums of maximums. This indicates that the initiation of charging with these catalysts is significantly different than that of VC or Au/C.

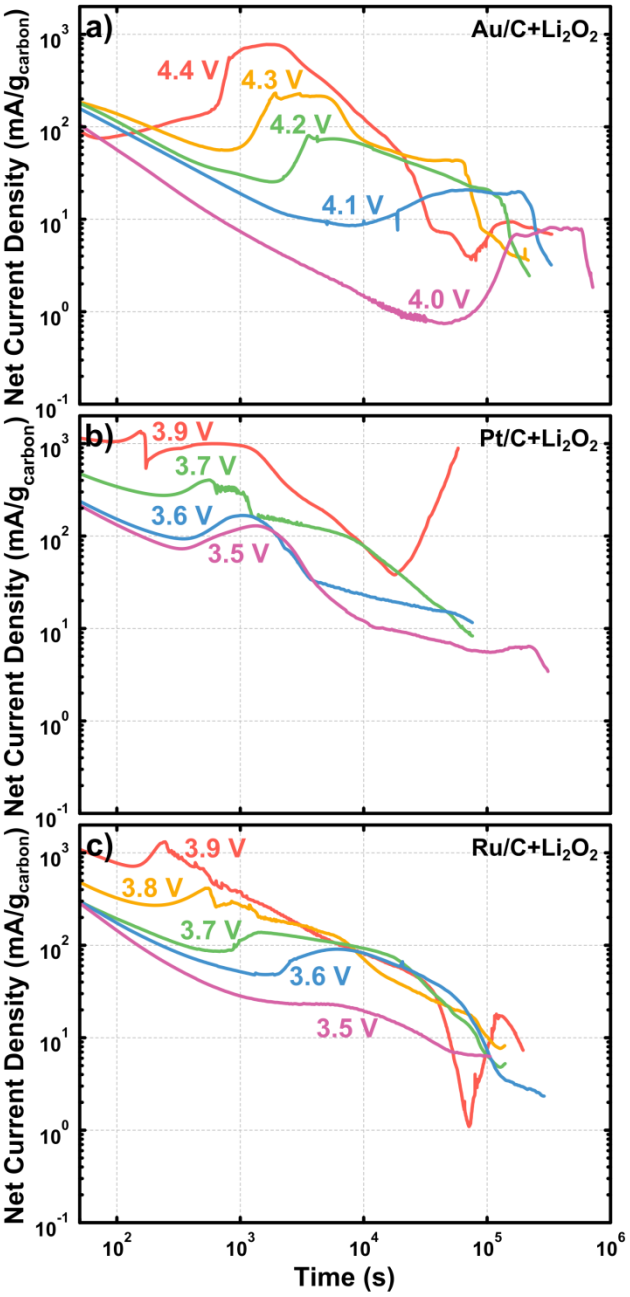

Fig. S11: Net current vs time on a log-log scale for (a) Au/C+Li_2O_2, (b) Pt/C+Li_2O_2, and (c) Ru/C+Li_2O_2

13. Capacity Variation of Electrodes

Slightly higher capacities were found in VC+Li_2O_2 cells with increasing potentials, which may suggest more complete oxidation of Li_2O_2 in the electrode and more electrolyte

oxidation, Cells charged at 4.5 V completed discharge in less than 10 hrs, while cells charged at 4.1 V took more than 50 hrs and cells charged at 4.0 V required more than 100 hrs to charge completely. This difference in time scales significantly increases the error from integration.

This same trend applies to Au/C+Li_2O_2 as well. The capacity was lowest at 4.0 V. For all cells at 4.1, 4.2, and 4.3 V, the capacity stayed within 10% of the expected capacity. At 4.4, the termination point was not as clearly defined and sometimes extended beyond the expected capacity. However, at this potential the background current was relatively high (~5 mAh/g_{carbon}), which limits the accuracy of net current calculations below 10 mAh/g_{carbon}. All of the excess charging in these cells stayed below this limit of 10 mAh/g_{carbon}.

14. References

1. B. D. McCloskey, R. Scheffler, A. Speidel, D. S. Bethune, R. M. Shelby and A. C. Luntz, *Journal of the American Chemical Society*, 2011, **133**, 18038-18041.
2. S. A. Freunberger, Y. H. Chen, N. E. Drewett, L. J. Hardwick, F. Barde and P. G. Bruce, *Angew Chem Int Edit*, 2011, **50**, 8609-8613.
3. Y. C. Lu, D. G. Kwabi, K. P. C. Yao, J. R. Harding, J. G. Zhou, L. Zuin and Y. Shao-Horn, *Energy & Environmental Science*, 2011, **4**, 2999-3007.
4. R. R. Mitchell, B. M. Gallant, C. V. Thompson and Y. Shao-Horn, *Energy & Environmental Science*, 2011, **4**, 2952-2958.